# Heterodyne moiré surface profilometry

**Wei-Yao Chang,[1] Fan-Hsi Hsu,[1] Kun-Huang Chen,[2,*] Jing-Heng Chen,[3] and Ken Y. Hsu[1]**

*[1]Department of Photonics and Institute of Electro-Optical Engineering, National Chiao Tung University, 1001 Ta-Hsueh Road, Hsinchu 30050, Taiwan*
*[2]Department of Electrical Engineering, Feng Chia University,100 Wenhwa Road, Seatwen, Taichung 40724, Taiwan*
*[3]Department of Photonics, Feng Chia University,100 Wenhwa Road, Seatwen, Taichung 40724, Taiwan*
*[*]chenkh@fcu.edu.tw*

**Abstract:** In this study, a novel moiré fringe analysis technique is proposed for measuring the surface profile of an object. After applying a relative displacement between two gratings at a constant velocity, every pixel of CMOS camera can capture a heterodyne moiré signal. The precise phase distribution of the moiré fringes can be extracted using a one-dimensional fast Fourier transform (FFT) analysis on every pixel, simultaneously filtering the harmonic noise of the moiré fringes. Finally, the surface profile of the tested objected can be generated by substituting the phase distribution into the relevant equation. The findings demonstrate the feasibility of this measuring method, and the measurement error was approximately 4.3 μm. The proposed method exhibits the merits of the Talbot effect, projection moiré method, FFT analysis, and heterodyne interferometry.



**OCIS codes:** (120.4120) Moiré techniques; (120.6650) Surface measurements, figure; (070.6760) Talbot and self-imaging effects; (040.2840) Heterodyne.

## References and links

1. H. Takasaki, "Moiré topography from its birth to practical application," Opt. Lasers Eng. **3**(1), 3–14 (1982).
2. J. J. J. Dirckx, W. F. Decraemer, and G. Dielis, "Phase shift method based on object translation for full field automatic 3-D surface reconstruction from moire topograms," Appl. Opt. **27**(6), 1164–1169 (1988).
3. A. A. Mudassar and S. Butt, "Self-imaging-based laser collimation testing technique," Appl. Opt. **49**(31), 6057–6062 (2010).
4. J. Dhanotia and S. Prakash, "Automated collimation testing by incorporating the Fourier transform method in Talbot interferometry," Appl. Opt. **50**(10), 1446–1452 (2011).
5. J. Y. Lee, Y. H. Wang, L. J. Lai, Y. J. Lin, and Y. H. Chang, "Development of an auto-focus system based on the moiré method," Measurement **44**(10), 1793–1800 (2011).
6. Y. Nakano and K. Murata, "Talbot interferometry for measuring the focal length of a lens," Appl. Opt. **24**(19), 3162–3166 (1985).
7. M. de Angelis, S. De Nicola, P. Ferraro, A. Finizio, and G. Pierattini, "A new approach to high accuracy measurement of the focal lengths of lenses using a digital Fourier transform," Opt. Commun. **136**(5-6), 370–374 (1997).
8. M. Ramulu, P. Labossiere, and T. Greenwell, "Elastic–plastic stress/strain response of friction stir-welded titanium butt joints using moiré interferometry," Opt. Lasers Eng. **48**(3), 385–392 (2010).
9. K. S. Lee, C. J. Tang, H. C. Chen, and C. C. Lee, "Measurement of stress in aluminum film coated on a flexible substrate by the shadow moiré method," Appl. Opt. **47**(13), C315–C318 (2008).
10. M. Takeda, H. Ina, and S. Kobayashi, "Fourier-transform method of fringe-pattern analysis for computer-based topography and interferometry," J. Opt. Soc. Am. **72**(1), 156–160 (1982).
11. Y. M. He, C. J. Tay, and H. M. Shang, "Deformation and profile measurement using the digital projection grating method," Opt. Lasers Eng. **30**(5), 367–377 (1998).
12. S. Mirza and C. Shakher, "Surface profiling using phase shifting Talbot interferometric technique," Opt. Eng. **44**(1), 013601 (2005).
13. C. Quan, Y. Fu, and C. J. Tay, "Determination of surface contour by temporal analysis of shadow moiré fringes," Opt. Commun. **230**(1-3), 23–33 (2004).
14. Y. B. Choi and S. W. Kim, "Phase-shifting grating projection moiré topography," Opt. Eng. **37**(3), 1005–1010 (1998).
15. J. A. N. Buytaert and J. J. J. Dirckx, "Design considerations in projection phase-shift moiré topography based on theoretical analysis of fringe formation," J. Opt. Soc. Am. A **24**(7), 2003–2013 (2007).
16. J. A. N. Buytaert and J. J. J. Dirckx, "Moiré profilometry using liquid crystals for projection and demodulation," Opt. Express **16**(1), 179–193 (2008).

#200100 - $15.00 USD Received 24 Oct 2013; revised 20 Jan 2014; accepted 29 Jan 2014; published 31 Jan 2014

17. J. J. J. Dirckx, J. A. N. Buytaert, and S. A. M. Van Der Jeught, "Implementation of phase-shifting moire profilometry on a low-cost commercial data projector," Opt. Lasers Eng. **48**(2), 244–250 (2010).
18. J. A. N. Buytaert and J. J. J. Dirckx, "Study of the performance of 84 phase-shifting algorithms for interferometry," J. Opt. **40**(3), 114–131 (2011).
19. M. Testorf, J. Jahns, N. A. Khilo, and A. M. Goncharenko, "Talbot effect for oblique angle of light propagation," Opt. Commun. **129**(3-4), 167–172 (1996).
20. D. C. Su, M. H. Chiu, and C. D. Chen, "A heterodyne interferometer using an electro-optic modulator for measuring small displacement," J. Opt. **27**(1), 19–23 (1996).

## 1. Introduction

The moiré measurement technique involves a simple optical apparatus; it is stable, economical, and can be used in a large measurement range; therefore, it has been widely employed in surface profile measurements [1, 2], light beam collimation tests [3, 4], auto-focus tests [5], focal length measurements [6, 7], and stress measurements [8, 9]. In moiré surface profilometry, the information related to the tested surface profile can be recorded in the moiré fringes; thus, the capability of the moiré fringe analysis technique strongly affects the precision and resolution of the measurement, and whether the relevant information involved in the moiré fringes can be completely extracted. Moiré fringe analysis techniques, like the interferometric fringe analysis of the optical interferometer, can be divided into two primary groups, the Fourier transform methods [10, 11] and phase-shift methods [12–18]. However, the harmonic noise which results from the grating lines spreads throughout the whole moiré fringes, and eliminating this noise is a critical concern when conducting moiré fringe analysis. The procedure for filtering harmonic noise in the Fourier transform methods involves a mathematical calculation in the frequency domain; however, because it is difficult to determine a precise spatial carrier frequency for the moiré fringes, shifting the frequency to remove the carrier frequency is difficult and can generate substantial measurement errors. Additionally, when the height distribution of the tested surface sharply changes, resulting in dramatic changes in the phase map, detailed information regarding the moiré fringe can be filtered out when filtering the spectra of the background light and harmonic noise. In the phase-shift methods, Mirza et al. [12] and Quan et al. [13] eliminated the harmonic noise in moiré images by filtering at every phase-shift step. Because this procedure is an approximate approach, the resulting information regarding the surface profile may lack detail. Choi et al. [14] and Buytaert et al. [15–17] used an optical compensation technique in phase-shift method to filter out the grating noise, and the use of DFT to extract the moiré phase is further explained by Buytaert et al. [18]. This technique synchronously moved two gratings, displacing one grating pitch per phase-shift step and setting the moving time as the exposure time of the camera; repeating this at every phase-shift step removed the harmonic noise. This strategy can be used to extract comprehensive information regarding moiré fringes. Though these controlling and matching procedures are trivial, but the outstanding measurement performance can still be carried out by a precise automatic control system. Beside, Although the previous researches have proposed many excellent approaches and outstanding results, we still attempt to improve the accuracy in Fourier transform method and some phase shifting methods which filter the moiré images in every phase step, and further to reduce the recording time and the probable errors that may be introduced from the controlling and matching process in the optical compensation. Therefore, a novel approach is proposed for measuring surface profiles that involves analyzing the heterodyne moiré signals pixel-by-pixel by using one-dimensional fast Fourier transform (FFT); this allows the harmonic noise of the moiré fringe to be filtered, requiring less recording time, but yielding detailed information regarding the tested surface profile. To validate the feasibility of the proposed method, the surface profile of a coin was measured. The measurement error was approximately 4.3 μm. Because it integrates the Talbot effect, projection moiré, FFT analysis, and heterodyne interferometry, the proposed method attains high precision, high resolution, high stability, and can be used in a large measurement range.

#200100 - $15.00 USD Received 24 Oct 2013; revised 20 Jan 2014; accepted 29 Jan 2014; published 31 Jan 2014

## 2. Principle

Figure 1 shows the optical configuration of the proposed approach. For convenience, the *z*-axis is assigned as the observation axis of the CMOS camera C, and the *y*-axis is set perpendicular to the paper plane. A laser light beam (wavelength $\lambda$) passes through a beam expander to form an expanded and collimated light beam. Subsequently, the light beam impinges on linear grating $G_1$ at projection angle $\alpha$ forming a self-image of grating $G_1$ and projecting the first self-image on the test surface. The first self-image distance $Z_1$ can be expressed as follows [19]:

$$Z_1 = \frac{p^2}{\lambda}\cos^3\alpha, \tag{1}$$

where $p$ is the pitch of grating $G_1$. The projected fringes are deformed because of the surface profile; this can be expressed as follows:

$$q_1(x,y) = \frac{1}{2}\left\{1+\gamma\cos\left[\frac{2\pi}{p}\left(-x-z(x,y)\tan(-\alpha)\right)-\phi_1\right]\right\}, \tag{2}$$

where $\gamma$ is the visibility of the deformed fringes, $z(x, y)$ is the height distribution of the tested surface, and $\phi_1$ is the initial phase of grating $G_1$. The deformed fringes are imaged at 1 × magnification on reference grating $G_2$ with a grating pitch of $p$ to form the moiré fringes; the image was captured using a CMOS camera C. The captured fringes can be expressed as follows:

$$\begin{aligned} q_2(x,y) &= q_1(-x,-y)\times W(x,y) \\ &= \frac{1}{2}\left\{1+\gamma\cos\left[\frac{2\pi}{p}\left(x+z(-x,-y)\tan\alpha\right)+\phi_1\right]\right\}\times\frac{1}{2}\left[1+\cos\left(\frac{2\pi}{p}x+\phi_2\right)\right], \end{aligned} \tag{3}$$

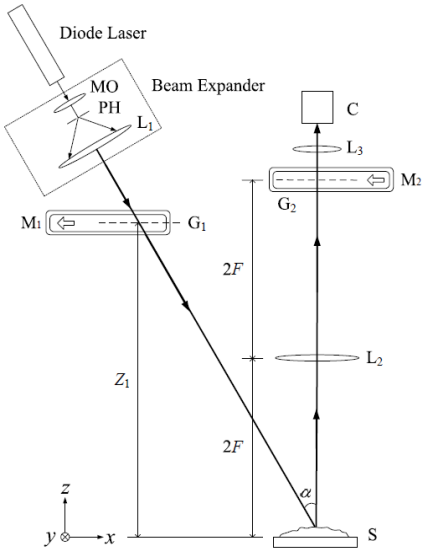


Fig. 1. Optical configuration. MO: microscopic objective; PH: pinhole; $L_1$: collimating lens; $L_2$: imaging lens; $L_3$: camera lens; $G_1$ and $G_2$: linear gratings; $M_1$ and $M_2$: translation motorized stage; C: CMOS camera; $Z_1$: first Talbot distance; $F$: focal length of imaging lens; $\alpha$: projection angle; S: sample.

#200100 - $15.00 USD Received 24 Oct 2013; revised 20 Jan 2014; accepted 29 Jan 2014; published 31 Jan 2014

where $q_1(-x, -y)$ denotes the imaging fringes of $q_1(x, y)$ by using the imaging lens $L_2$; $W(x, y)$ is the transmission function of grating $G_2$; and $\phi_2$ is the initial phase of grating $G_2$. Equation (3) can be written as follows:

$$q_2(x,y)=\frac{1}{4}\left\{1+\gamma\cos\left[\frac{2\pi}{p}\left(x+z(-x,-y)\tan\alpha\right)+\phi_1\right]+\cos\left(\frac{2\pi}{p}x+\phi_2\right)\right.$$
$$\left.+\frac{\gamma}{2}\cos\left[\frac{2\pi}{p}\left(2x+z(-x,-y)\tan\alpha\right)+\phi_1+\phi_2\right]+\frac{\gamma}{2}\cos\left[\phi(x,y)+\phi_1-\phi_2\right]\right\}, \quad (4)$$

and

$$\phi(x,y)=\frac{2\pi\tan\alpha}{p}\cdot z(-x,-y), \quad (5)$$

where $\phi(x, y)$ is the phase distribution of the moiré fringes. In Eq. (4), the second, third, and fourth terms are the harmonic noise, and the last term is the moiré fringe, which is primarily relative to the height distribution of the tested surface. To obtain the phase distribution $\phi$, gratings $G_1$ and $G_2$ are moved at a constant speed, $v$ along the $-x$-direction by using the motorized translation stages $M_1$ and $M_2$, respectively. Thus, every pixel of the CMOS camera C can receive the time-varying signal and the moiré fringes can be expressed as follows:

$$q_3(t,x,y)=q_1(t,-x,-y)\times W(t,x,y)$$
$$=\frac{1}{2}\left\{1+\gamma\cos\left[2\pi f_0 t+\frac{2\pi x}{p}+\phi+\phi_1\right]\right\}\times\frac{1}{2}\left[1+\cos\left(2\pi(-f_0)t+\frac{2\pi x}{p}+\phi_2\right)\right], \quad (6)$$

where $f_0 = v/p$ is the frequency introduced by the grating movement. Equation (6) can be rewritten as:

$$q_3(t,x,y)=\frac{1}{4}\left\{1+\gamma\cos\left(2\pi f_0 t+\frac{2\pi x}{p}+\phi+\phi_1\right)+\cos\left[2\pi(-f_0)t+\frac{2\pi x}{p}+\phi_2\right]\right.$$
$$\left.+\frac{\gamma}{2}\cos\left(\frac{4\pi x}{p}+\phi+\phi_1+\phi_2\right)+\frac{\gamma}{2}\cos\left(2\pi f_h t+\phi+\phi_1-\phi_2\right)\right\}, \quad (7)$$

where the last term is not relative to the grating line along the $x$-direction and $f_h = 2f_0$ is the heterodyne moiré frequency. For convenience, Eq. (7) can be rewritten using the Euler formula as follows [10]:

$$q_3(t,x,y)=\frac{1}{8}\left\{\left[a(t,x,y)+a^*(t,x,y)\right]+\left[b(t,x,y)\cdot\exp\left(i2\pi f_0 t\right)+b^*(t,x,y)\cdot\exp\left(-i2\pi f_0 t\right)\right]\right.$$
$$+\left[c(t,x,y)\cdot\exp\left[i2\pi(-f_0)t\right]+c^*(t,x,y)\cdot\exp\left[i2\pi(-f_0)t\right]\right]$$
$$\left.+\frac{1}{2}\left[d(t,x,y)\cdot\exp\left(i2\pi f_h t\right)+d^*(t,x,y)\cdot\exp\left(-i2\pi f_h t\right)\right]\right\}, \quad (8)$$

where * denotes the complex conjugate operator, and

$$a(t,x,y)=1+\frac{\gamma}{2}\exp\left[i\left(\frac{4\pi x}{p}\right)+\phi+\phi_1+\phi_2\right], \quad (9)$$

#200100 - $15.00 USD Received 24 Oct 2013; revised 20 Jan 2014; accepted 29 Jan 2014; published 31 Jan 2014

$$b(t,x,y)=\gamma\exp\left[i\left(\frac{2\pi x}{p}+\phi+\phi_1\right)\right], \tag{10}$$

$$c(t,x,y)=\frac{\gamma}{2}\exp\left[i\left(\frac{2\pi x}{p}+\phi_2\right)\right], \text{ and} \tag{11}$$

$$d(t,x,y)=\frac{\gamma}{2}\exp\left[i\left(\phi+\phi_1-\phi_2\right)\right]. \tag{12}$$

Applying the FFT to Eq. (8), Eq. (13) yields the following:

$$Q(f,x,y)=\frac{1}{8}\Big\{A(f,x,y)+A^*(f,x,y)+B(f-f_0,x,y)+B^*(f+f_0,x,y) +\frac{1}{2}\left[C(f+f_0,x,y)+C^*(f-f_0,x,y)\right]+\frac{1}{2}\left[D(f-f_h,x,y)+D^*(f+f_h,x,y)\right]\Big\}, \tag{13}$$

where $Q$, $A$, $B$, $C$, and $D$ are the Fourier transform of $q_3$, $a$, $b$, $c$, and $d$. Subsequently, $D(f-f_h, x, y)$ is shifted to $D(f, x, y)$ and processed using the inverse Fourier transform to obtain $d(t, x, y)$. Calculating a logarithm of $d(t, x, y)$ yields:

$$\ln\left[d(x,y)\right]=\ln\left(\frac{\gamma}{2}\right)+i\left(\phi+\phi_1-\phi_2\right). \tag{14}$$

Extracting the imaginary part of Eq. (14) allows generating $\phi + \phi_1-\phi_2$. To generate phase distribution $\phi(x, y)$, this procedure was applied to every pixel of camera C, and the initial phase difference $\phi_1-\phi_2$ was neglected because it did not influence the relative height distribution of the surface measurement. Considering the image reversal that results from the imaging lens, Eq. (5) can be rewritten as follows:

$$z(x,y)=\frac{p}{2\pi\cdot\tan\alpha}\cdot\phi(-x,-y). \tag{15}$$

Finally, substituting $\phi(x, y)$ into Eq. (15) and considering the image reversal that resulted from the imaging lens, the surface profile of the tested object can be reconstructed.

## 3. Experimental results and discussions

To validate the feasibility of the proposed method, a coin was measured [Fig. 2(a)]. The experimental setup comprised a diode laser (wavelength = 473 nm), two linear gratings (pitch = 0.2822 mm), an imaging lens with a focal length of 200 mm, two motorized translation stages (Sigma Koki/SGSP(MS)26 −100) with resolution of 0.05 μm to generate a heterodyne frequency $f_h$ = 20 Hz ($v$ = 0.2822 mm/s), and a CMOS camera (Basler /A504k) with an 8-bit gray level and 1280 × 1024 image resolution. For convenience, the projection angle was set at 30°, the frame rate of the CMOS camera was set at $f_s$ = 120 fps, the exposure time was set at $t_e$ = 8 ms, and the total recording time was set at $T$ = 1 s to record the heterodyne moiré signals at various times. Figures 2(b)-2(d) display the experimental results. Figure 2(b) is a recorded moiré image, showing that grating noise spread throughout the image. Despite the nonuniform light intensity distribution, nonuniform scattering property of the coin surface, and the height distribution of the coin, which is lower than that one period of the moiré fringe can represent, the phase distribution of the moiré fringes were extracted by using the proposed fringe analysis method [Fig. 2(c)]. The surface profile of the coin was reconstructed using Eq. (15), as shown in Fig. 2(d). To prove the accuracy of the proposed method, the

#200100 - $15.00 USD Received 24 Oct 2013; revised 20 Jan 2014; accepted 29 Jan 2014; published 31 Jan 2014

contour from A to A′ [Fig. 2(a)] was measured using a stylus profilometer (KLA-Tencor/Alpha Step D-100) to

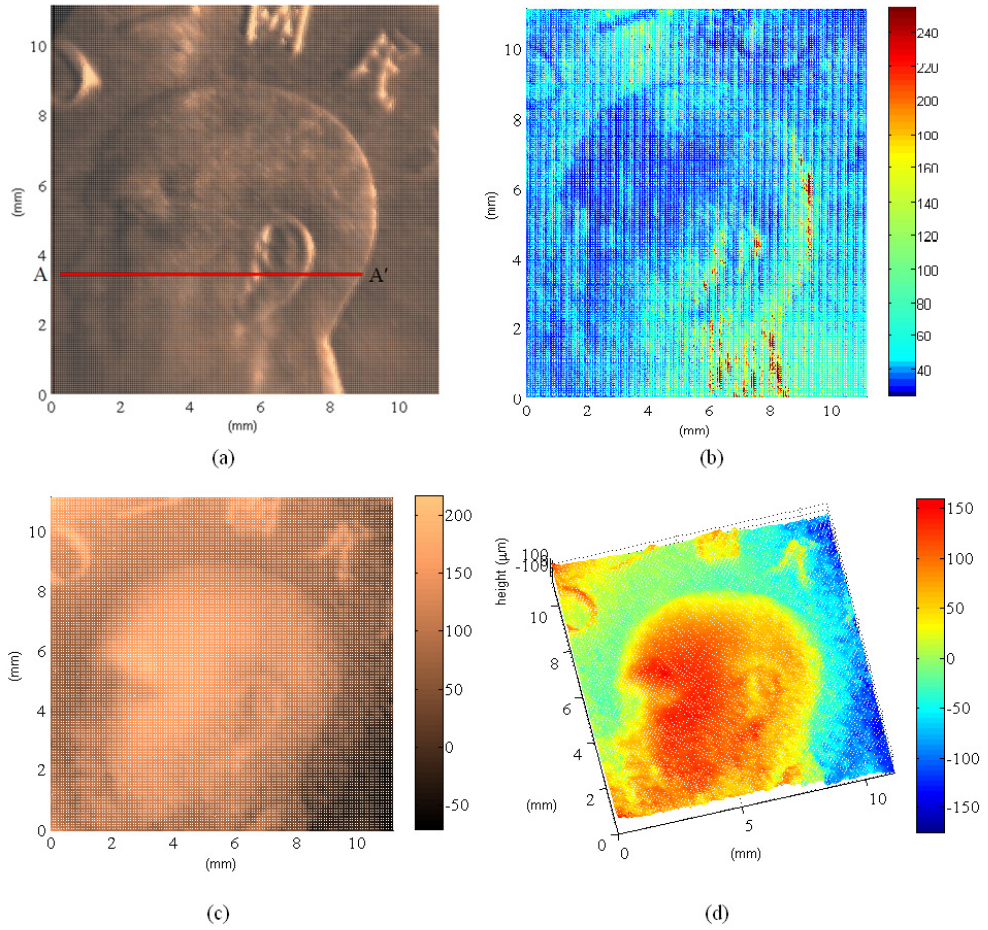


Fig. 2. Sample image and experimental results. (a) coin image; (b) moiré fringes on coin surface; (c) phase map of moiré fringes on coin surface.; (d) reconstructed coin surface profile.

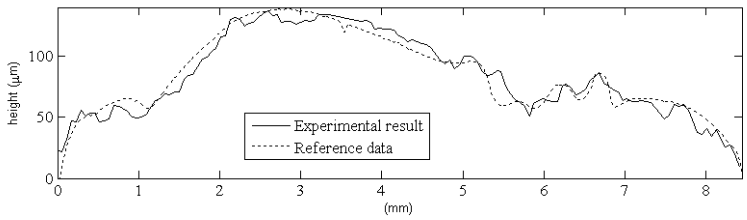


Fig. 3. Contour lines depicted from experimental and reference data.

serve as reference data. Figure 3 shows the contour lines from the experimental and reference data, indicating that the experimental and reference data exhibited the same height trends; this proves the feasibility of the proposed method.

According to Eq. (6), the height error Δz yielded by using the proposed method can be expressed as follows:

#200100 - $15.00 USD Received 24 Oct 2013; revised 20 Jan 2014; accepted 29 Jan 2014; published 31 Jan 2014

$$\Delta z = \left|\frac{\partial z}{\partial p}\Delta p\right| + \left|\frac{\partial z}{\partial \alpha}\Delta \alpha\right| + \left|\frac{\partial z}{\partial \phi}\Delta \phi\right|, \tag{16}$$

where $\Delta p$ is the grating pitch error, $\Delta \alpha$ is the projection angle error, and $\Delta \phi$ is the phase error. The grating pitch error resulted from fabrication error. Because the gratings in the experiment were produced by plating chromium on a glass plate using a mask laser writer, the grating pitch error $\Delta p$ was approximately 0.1 μm. The projection angle error resulted from axis alignment error and the resolution of the rotary stage. When the axis alignment error was 0.05° and the resolution of the rotary stage was 10 arcmin, the projection angle error $\Delta \alpha$ was approximately 0.22°. The phase error of the proposed method primarily resulted from the sampling error. When heterodyne moiré signals are captured using a CMOS camera, using an exposure and integration process, the recorded intensity of one pixel at the $k$th sampling point can be expressed as follows:

$$\begin{aligned} q_c(kt_s) = \frac{1}{t_e}\int_{kt_s}^{kt_s+t_e} q_3 \cdot dt = \frac{1}{4}\Bigg\{ & 1 + \gamma \sin c(f_0 t_e)\cos\left(2\pi f_0 k t_s + \frac{2\pi x}{p} + \phi + \phi_1 + \pi f_0 t_e\right) \\ & + \sin c(-f_0 t_e)\cos\left[2\pi(-f_0)kt_s + \frac{2\pi x}{p} + \phi_2 + \pi f_0 t_e\right] + \frac{\gamma}{2}\cos\left(\frac{4\pi x}{p} + \phi + \phi_1 + \phi_2\right) \\ & + \frac{\gamma}{2}\sin c(f_h t_e)\cos\left[2\pi(f_h)kt_s + \phi + \phi_1 - \phi_2 + \pi f_h t_e\right]\Bigg\}, \end{aligned} \tag{17}$$

where $t_s = 1/f_s$ is the frame period. The intensity is subsequently quantized in gray-level units as:

$$q_d(kt_s) = round\left(q_c \times 2^n\right), \tag{18}$$

where $n$ denotes the number of the gray level. After substituting the experimental conditions in Eqs. (17) and (18), the captured heterodyne moiré signal of one pixel can be simulated and analyzed using FFT. The phase error $\Delta \phi$ can be obtained by comparing the calculated phases of FFT and set $\phi$ when the relative phase measurement of the surface profilometry is considered and the light intensity error resulting from the stability of the light source and grating vibration is 1%. The phase error $\Delta \phi$ of the proposed method can be estimated as approximately 1.53°. Substituting the experimental conditions, $\Delta p$, $\Delta \alpha$, and $\Delta \phi$ into Eq. (16) yielded a height error $\Delta z$ of approximately 4.3 μm.

The visibility of the projected fringes influences the amplitude of heterodyne moiré signals, and affects the recorded magnitude of heterodyne frequency component, namely $d(x, y)$ in Eq. (12). It is obvious that if visibility is zero, the heterodyne frequency component and the phase of this component certainly cannot be extracted by FFT. Therefore, the suggested minimum visibility is about 0.4 because the height error in this condition reaches 6.67 μm. The lower visibility causes much larger height error and results in a disappointing result. Besides, the angular misalignment between the directions of the projected fringes and the grating line of $G_2$ can reach 0.01 arcmin in our experiment. The resultant phase variation caused by this small angle in whole image can be estimated merely within $1.7 \times 10^{-5}$ degree [4], hence the resultant small angular misalignment can be neglected.

The proposed heterodyne moiré interferometry is analogous to the conventional heterodyne interferometry [20]. The heterodyne moiré frequency is introduced by the beat frequency between two grating movement frequencies, and analyzing the heterodyne moiré signal can achieve the measurement purpose. In addition, according to the principle, the experimental results, and the error analysis, the proposed method can avoid losing the detail information of moiré fringes because the grating noise is filtered out pixel by pixel. Hence,

#200100 - $15.00 USD Received 24 Oct 2013; revised 20 Jan 2014; accepted 29 Jan 2014; published 31 Jan 2014

this approach has higher accuracy than the techniques that filter out the grating noise in spatial frequency domain, such as conventional Fourier transform method whose maximum detectable spatial frequency on the surface is limited by the spatial frequency of the carrier fringes or the grating noise [10], and some phase shifting methods which filter the moiré images in every phase step. Besides, phase shifting method combined with the optical compensation method is a powerful technique to filter out the grating noise of moiré and to extract the accurate phase data. However, this approach can just be implemented by continuously moving two gratings in a time interval and recording continuously time-varying signals. Analyzing the captured signals can filter out the grating noise and extract the phase data at the same time. Therefore, the proposed method can avoid the probable errors that may be introduced when controlling and matching the displacement of motorized translation stage and the exposure time of camera in the optical compensation. Furthermore, the recording time of this method is less than the optical-compensation phase shifting method in the same conditions of the grating speed and the frame rate of camera. Hence, the proposed method has higher stability due to the less measurement time. It is worthy to mention that applying spatial light modulator or LCD projector to moiré profilometry has been developed to improve the instability caused from the mechanical vibration [16, 17].

## 4. Conclusion

A novel moiré fringe analysis technique is proposed for measuring the surface profile of an object, integrating the Talbot effect, projection moiré method, FFT analysis, and heterodyne interferometry. To validate the proposed approach, a coin was measured, yielding a height error of approximately 4.3 μm. Because the grating noise is filtered out pixel by pixel, the proposed method can avoid losing the detail information of moiré fringes. This approach can just analyze the recorded continuously time-varying signals to simultaneously filter out the grating noise and to extract the phase data, hence it can reduce the probable errors resulted from controlling and matching procedures. Additionally, this method demonstrates the advantages of the combined techniques, yielding high precision, high resolution, high stability, and applicability in a large measurement range.

## Acknowledgments

The authors would like to thank the National Science Council of the Republic of China, Taiwan for financially supporting this research under Contract No. NSC 101-2221-E-009-112-MY3 and NSC 102-2221-E-035-057.

#200100 - $15.00 USD Received 24 Oct 2013; revised 20 Jan 2014; accepted 29 Jan 2014; published 31 Jan 2014